Turbulence near cyclic fold bifurcations in birhythmic media

Dorjsuren Battogtokh* and John J. Tyson
Department of Biology, Virginia Polytechnic Institute and State University, Blacksburg, Virginia 24061-0106, USA
(Received 23 February 2004; published 26 August 2004)

We show that at the onset of a cyclic fold bifurcation, a birhythmic medium composed of glycolytic oscillators displays turbulent dynamics. By computing the largest Lyapunov exponent, the spatial correlation function, and the average transient lifetime, we classify it as weak turbulence of a transient nature. Virtual heterogeneities generating unstable fast oscillations account for the transient turbulence. In the presence of a wave number instability, unstable oscillations can be reinjected, leading to stationary turbulence. We also find similar turbulence in a cell cycle model. These findings suggest that weak turbulence may be universal in biochemical birhythmic media exhibiting cyclic fold bifurcations.

DOI: 10.1103/PhysRevE.70.026212 PACS number(s): 05.45.Jn, 05.45.Pq, 82.39.Fk, 82.40.Bj

I. INTRODUCTION

In studies of chemical turbulence in reaction diffusion systems near a Hopf bifurcation, a reduction of the model to the complex Ginzburg-Landau equation (CGLE) is very useful [1,2]. First, it allows one to determine a parameter set in the model leading to turbulence without carrying out extensive simulations [3]. Second, the detailed knowledge of the CGLE's dynamics can be very helpful [4–8], because mathematical models from different disciplines displaying dynamics near a Hopf bifurcation obey the same qualitative dynamics of the CGLE [9].

However, the CGLE alone is insufficient for a qualitative description of realistic models in a neighborhood of a Hopf bifurcation, when other bifurcations occur nearby [10,11]. For example, near a supercritical Hopf bifurcation point, another stable limit cycle may exist, so that, depending on initial conditions, oscillations with two different frequencies and amplitudes are possible. Such a situation, called birhythmicity, is a characteristic feature of a number of well-known models of biochemical oscillations [14,15]. For these systems, the CGLE cannot be used without appropriate modifications. Often, the best way to approach these problems is by simulations of the original models [11,12].

To the best of our knowledge, little is known about turbulence in birhythmic media. Intuitively, in a regime of strong wave number instability, birhythmicity should not be a factor. Therefore, turbulence in homogeneous birhythmic media and in coupled limit cycle oscillators should have similar characteristics. In the absence of wave number instability, high-frequency oscillations are supposed to suppress slow oscillations and restore uniform oscillations. But at the onset of a cyclic fold (CF) bifurcation in birhythmic media of a biochemical origin, high-frequency oscillations may be unstable. Thus, a complete suppression of slow oscillations may not be achieved in these systems. On the contrary, if unstable oscillations emerge persistently, complex spatiotemporal motions are possible.

The goal of this work is to show that near cyclic fold bifurcations in birhythmic media, virtual heterogeneities creating unstable oscillations can lead to a peculiar turbulence, intermittency of small- and large-amplitude oscillations. We will first compute complex spatiotemporal behavior in a birhythmic medium composed of glycolytic oscillators. By calculating the maximal Lyapunov exponent, the spatial correlation function, and the average transient lifetime, we will provide evidence that this behavior is weak transient turbulence. In the presence of a wave number instability, transient turbulence may become stationary. Mathematically, the instability of the faster oscillations is a result of a CF bifurcation driven by the terms representing enzymatic regulations, suggesting that weak turbulence may be common in biochemical birhythmic media exhibiting CF bifurcations. As further evidence, we demonstrate weak turbulence in a cell cycle model. A biological system where weak turbulence might possibly be found is presented in the closing section.

II. BIRHYTHMIC MEDIUM OF GLYCOLYTIC OSCILLATORS

Let us introduce a birythmic medium composed of glycolytic oscillators:

$$\frac{d\alpha}{dt} = \nu + \frac{\sigma_i \gamma^n}{K^n + \gamma^n} - \sigma\phi + D_\alpha \Delta\alpha, \tag{1}$$

$$\frac{d\gamma}{dt} = Q\sigma\phi - k_s\gamma - \frac{Q\sigma_i\gamma^n}{K^n + \gamma^n} + D_\gamma \Delta\gamma, \tag{2}$$

$$\phi = \frac{\alpha(1+\alpha)(1+\gamma)^2}{L + (1+\alpha)^2(1+\gamma)^2}.$$

In Eqs. (1) and (2), α and γ represent dimensionless substrate and product concentrations of glycolytic reactions; K, n, ν, σ_i, σ, k_s, L, and Q are parameters (all $\geqslant 0$). For convenience, we assume $Q \equiv 1$ throughout this paper. D_α and D_γ are diffusion constants for the substrate and product. We define time and space units in Eqs. (1) and (2) in sec and cm, respectively. When $D_\alpha = 0$, $D_\gamma = 0$, and $\sigma_i = 0$, Eqs. (1) and (2) are called the glycolytic oscillator [14]. The term $\sigma_i\gamma^n/(K^n + \gamma^n)$ represents substrate recycling that drives birhythmicity. Recently, in Ref. [16], Eqs. (1) and (2) were shown to sup-

*Electronic address: dbattogt@vt.edu

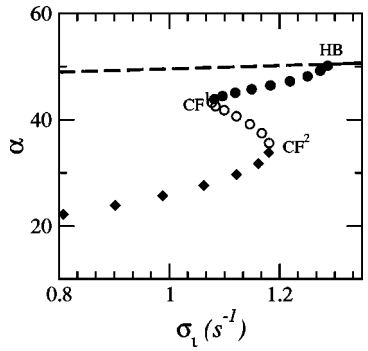

FIG. 1. A bifurcation diagram of Eqs. (1) and (2). *HB* marks a Hopf bifurcation point, $CF^{1,2}$ mark cyclic fold bifurcations. Parameters are $\nu=0.25\ s^{-1}$, $n=4$, $K=11.5$, $\sigma=11\ s^{-1}$, $k_s=0.05\ s^{-1}$, and $L=3\ 400\ 000$.

port multiple wave fronts. Our concern in this paper is a different parameter region where irregular spatiotemporal motions develop.

A phase plane analysis of Eqs. (1) and (2) shows that the mechanism of birhythmicity is two regions of negative slope in the product nullcline [14]. A convenient way to illustrate birhythmicity is with a bifurcation diagram. We used a well-known software package AUTO [17] for bifurcation analysis of the local model [$D_\alpha=D_\gamma=0$ in Eqs. (1) and (2)]. Solid lines in Fig. 1 show stable steady states, and dashed lines show unstable steady states. Stable limit cycles are shown by solid symbols, unstable limit cycles by open circles. Solid circles represent small-amplitude oscillations with high frequencies. Large-amplitude oscillations with lower frequencies are shown by solid diamonds in Fig. 1. A Hopf bifurcation point *HB* is located at $\sigma_{i,cr}\approx 1.282$. There are two CF bifurcations in Fig. 1, where stable limit cycles are replaced by unstable ones. Between these two CF points, which occur at $\sigma_{i,CF^1}\approx 1.077$ and $\sigma_{i,CF^2}\approx 1.183$, two stable limit cycles coexist. Therefore, depending on initial conditions, one of the limit cycles will be selected in simulations of the glycolytic oscillator with substrate recycling.

A general mechanism of turbulence in oscillatory reaction diffusion systems is wave number instability—i.e., instability of uniform oscillations against phaselike fluctuations [1]. In Eqs. (1) and (2), there are two different uniform oscillations that might undergo wave number instability. We want to provide evidence that these oscillations are stable against phaselike fluctuations for the parameters in Fig. 1. For the fast, uniform oscillations which originate from the Hopf bifurcation point shown by solid circles in Fig. 1, the stability condition can be obtained by reducing Eqs. (1) and (2) to the CGLE

$$\dot{A} = (1 + ic_0)A - (1 + ic_2)|A|^2A + (1 + ic_1)\Delta A. \qquad (3)$$

In Eq. (3), A is the complex amplitude, and c_0, c_1, and c_2 are real parameters. The CGLE has a uniform oscillatory solution, $A=\exp[i(c_0-c_2)t]$, which is stable if the condition $1+c_1c_2>0$ holds. In the Appendix, we calculated c_0, c_1, and c_2 corresponding to Eqs. (1) and (2). Our results show that the uniform oscillations are stable for the parameters used in Fig. 1, or any $D_\alpha>0$ and $D_\gamma>0$. For $D_\alpha=D_\gamma$ we find that $c_1=0$. Hence, the parameter region we are interested in is deep inside the Benjamin-Feir stability region given by $1+c_1c_2>0$. Although the CGLE is valid only near the *HB* point, it is likely that the uniform oscillations will remain stable until the the next bifurcation in the system—i.e., CF^1 in Fig. 1 [9]. Next, consider the uniform oscillations with low frequencies. Unlike the case of fast oscillations, no analytic approach is available in this case. Note that oscillations shown by solid circles and diamonds in Fig. 1 occur at the same parameters. Therefore, it is rather unlikely that the slow oscillations undergo wave number instability, contrary to the fast ones. Thus, we can assume that uniform, slow oscillations are also stable.

It is known that strong perturbations can switch oscillations from one stable orbit to another in the glycolytic model with substrate recycling [14]. Therefore, even if both uniform oscillations in Eqs. (1) and (2) are stable against wave number instability, strong perturbations can excite the system by switching the oscillations. This kind of excitability, however, will not lead to turbulence; in the parameter interval $[\sigma_{i,CF^1},\sigma_{i,CF^2}]$, the fast oscillations will suppress the slow ones as time progresses. But for $|\sigma_i-\sigma_{i,CF^1}|\ll 1$ where the fast oscillations become unstable, it is apparent that a complete suppression of slow oscillations is impossible. Here, because of complex interactions between stable, slow and unstable, fast oscillations, interesting spatiotemporal dynamics might develop. Therefore, we carried out a detailed numerical study in the neighborhood of CF^1.

III. WEAK TURBULENCE IN A BIRHYTHMIC MEDIUM OF GLYCOLYTIC OSCILLATORS

For numerical integrations of Eqs. (1) and (2) in one spatial dimension, we used the fourth-order Runge-Kutta method. Diffusion terms were approximated by the finite-difference method. Numerical parameters are $\delta x=0.005$ cm and $\delta t=0.05$ s. The system size is defined as $l=N\delta x$, where N is the number of spatial grid points. In this paper we present results for periodic boundary conditions, but we also tested the main results with no-flux boundary conditions. We also tested selected examples with smaller values of δx and δt for fixed l. Our simulations show that Eqs. (1) and (2) are sensitive to initial conditions. By choosing initial conditions as small perturbations of uniform, slow oscillations with large amplitudes, we found that these oscillations are stable for $\sigma_i<\sigma_{i,CF^2}$. But near and to the left of CF^1, uniform, fast oscillations with small amplitudes are found to be unstable. They spiral out from unstable orbits towards the orbit of stable, large-amplitude oscillations. For strong perturbations near the CF^1 bifurcation point, we found spatiotemporal irregular motions in Eqs. (1) and (2).

Figure 2 shows a gray scale plot of spatiotemporal dynamics in Eqs. (1) and (2). Oscillations between the white and black colors show large-amplitude oscillations displayed by $\gamma(x,t)$. There are also oscillations with higher frequency and smaller amplitude in Fig. 2. Because the latter ones are unstable, they cannot suppress large-amplitude domains. Although uniform, large-amplitude oscillations are stable against small fluctuations, phase slips created by strong ini-

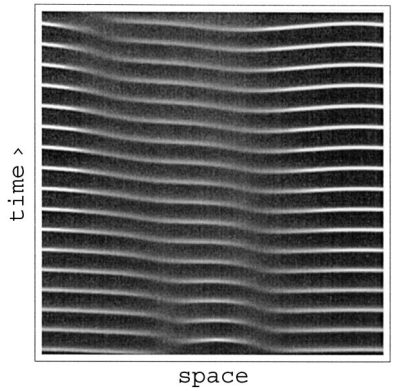

FIG. 2. Space-time pattern of γ in a weak turbulent regime of Eqs. (1) and (2). The space and time spans are $l=1.75$ cm and $T=5\times10^3$ s. The pattern was obtained by recording $\gamma(x)$ with a time interval $\tau=5$ s. $D_\alpha=D_\gamma=1\times10^{-5}$ cm^2/s and $\sigma_i=1.065$ s^{-1}. Other parameters are the same as in Fig. 1.

tial perturbations cannot be eliminated as time progresses. As a result, spatially nonuniform distributions of concentrations are seen at given time moments, Fig. 3. On the phase plane, these nonuniform distributions generate motions attracted by unstable orbits around the inner cycle shown in Fig. 4. We found that such unstable orbits act as a weak, virtual heterogeneity emerging randomly. They cannot entrain the bulk oscillations, but in their presence, phase slips cannot be eliminated. Instead, persistent spatiotemporal irregular motions develop.

To characterize the irregular motions in Fig. 2, we calculated the maximum Lyapunov exponent λ_{lyap}^{max} in $2N$-dimensional phase space [18]. First we made a very long run of Eqs. (1) and (2) to confirm that the turbulence is stationary. Then, by using the same initial conditions, we simulated Eqs. (1) and (2) and its linear system for computation of λ_{lyap}^{max} for $T_1=2\times10^5$ s. We found that the largest Lyaponov exponent is positive and small, $\lambda_{lyap}^{max}\approx2\times10^{-3}$. We also calculated a two-point correlation function $C(x)=\langle\gamma(x_0,t)\gamma(x_0+x,t)\rangle$, where $\langle\cdots\rangle$ stands for an average over space and time [19]. Figure 5 shows that $C(x)\approx$ const at small values of x, indicating strong local coupling and an absence of short waves. A power-law decay of the correlation function at intermediate values of x implies the presence of chaotic motions. We found that the slope is $\kappa\approx-0.15$. We

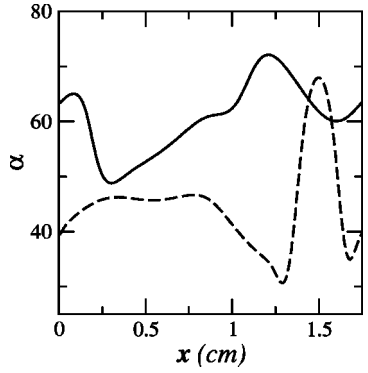

FIG. 3. Snapshots of spatial distributions of α at two different time moments. Parameters are the same as in Fig. 2.

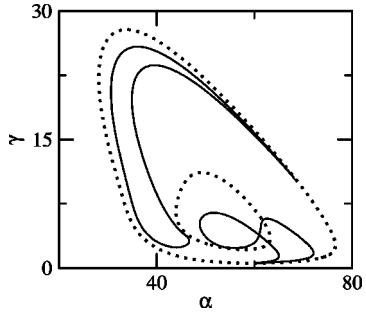

FIG. 4. A phase plane view. The outer cycle shows the orbit of stable uniform oscillations with a period $\tau=300$ s. The inner cycle shows the orbit of small-amplitude, fast oscillations with a period $\tau=290$ s at $\sigma_i=1.08$ s^{-1}. With the decrease of σ_i, the inner cycle disappears, but it still can attract neighboring trajectories, creating a virtual, chaotic heterogeneity in Eqs. (1) and (2). The solid lines show spatial distributions of oscillators projected onto the phase plane at two different time moments. Parameters are the same as in Fig. 2.

also found no significant variations of κ and λ_{lyap}^{max} with changes of σ_i and l. The small values of κ and $\lambda_{lyap}^{max}>0$ suggest that spatiotemporal irregular motions shown in Fig. 2–4 can be characterized as weak turbulence.

We found that in Eqs. (1) and (2), stationary irregular motions can develop only for certain initial conditions and system sizes. In simulations with different initial conditions and system sizes, we observed sudden collapses of the turbulent dynamics. The collapse of turbulence in Eqs. (1) and (2) means a complete suppression of small-amplitude oscillations. Thus, we defined the transient lifetime of turbulence, t_p, as the time interval from initial conditions to the moment when all oscillators come within a distance d of the orbit of stable, slow, large-amplitude oscillations. In our simulations we used $d=0.03$. Following Ref. [13], we plot an average transient lifetime t_p versus the system size l in Fig. 6. Here, each solid circle is an average of 20 simulations with different initial conditions. Figure 6 shows that, as the system size increases, t_p grows exponentially.

For some initial conditions, when l is close to 2 cm, the turbulent solution does not collapse. The inset in Fig. 6 shows the number of cases, among 20 different simulations, when a collapse of turbulence has not occurred by $T=10^6$ s. (These cases were not included in calculations of the solid circles in Fig. 6.) We continued two cases in the inset (at l

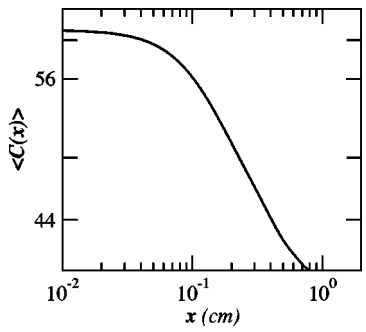

FIG. 5. A log-log plot of the spatial correlation function. Parameters are the same as in Fig. 2.

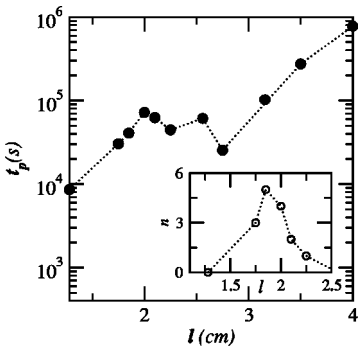

FIG. 6. Average transient lifetime versus the system size. The inset shows the cases when a collapse of turbulence has not occurred by $T=10^6$ s. Parameters are the same as in Fig. 2.

$=1.75$ cm) up to $T=10^8$ s and did not observe a collapse of motions near the inner cycle in Fig. 4.

Numerical experiments indicate that if virtual heterogeneities reside sufficiently far from each other, a stationary pattern is possible in the interval $\sigma_i \in [1.055, 1.075]$. Figure 7 gives an example of such a pattern. Here virtual heterogeneities are located from each other by distances between 0.5 and 1 cm. Note that these quasiperiodic structures are not related to a Turing instability, which emerges due to differences in diffusion coefficients. Unstable oscillations at the onset of a CF bifurcation are the instabilities leading to these structures. The cellular structures in Fig. 7 are breathing because of the unstable oscillations. Numerical results show that as the system size increases, the cells breath coherently.

A collapse of turbulence can be prevented if there is a reinjection mechanism for the unstable oscillations generated by the virtual heterogeneities. Naturally, wave number instability can be such a mechanism. Using our calculations in the Appendix, we simulated Eqs. (1) and (2) for parameters when the corresponding CGLE displays phase instability and found stationary weak turbulence for $|\sigma-\sigma_{i,CF^1}| \ll 1$.

IV. WEAK TURBULENCE IN A CELL CYCLE MODEL

In Sec. III, we demonstrated that the CF^1 bifurcation point is crucial for turbulence in Eqs. (1) and (2). Mathematically, the term representing substrate recycling drives CF bifurcations. In models of biochemical oscillations, terms representing enzymatic activities naturally arise. As an enzyme can quickly switch from being active to inactive and back again, ideal conditions for CF bifurcations exist in these models. Therefore, other biochemical reaction diffusion models may also display the weak turbulence discussed in the previous section. As an example, consider a three-variable model of the budding yeast cell cycle:

$$\frac{dX}{dt} = m(k_1 + k_2 T) - (k_3 + k_4 Y + k_5 Z)X + D_X \Delta X, \tag{4}$$

$$\frac{dY}{dt} = \frac{(k_6 + k_7 Z)(1 - Y)}{J_1 + 1 - Y} - \frac{(k_8 m + k_9 X)Y}{J_1 + Y} + D_Y \Delta Y, \tag{5}$$

$$\frac{dZ}{dt} = (k_{10} + k_{11} X) - k_{12} Z + D_Z \Delta Z, \tag{6}$$

$$T = G(X, P, J_2, J_2), \tag{7}$$

$$G(a,b,c,d) = \frac{2ad}{b - a + bc + ad + \sqrt{(b - a + bc + ad)^2 - 4ad(b - a)}}, \tag{8}$$

where the transcription factor T for X is given by the Goldbeter-Koshland function G [14]. X, Y, and Z are dimensionless variables and m is a dimensionless parameter. Time and space units in Eqs. (4)–(8) are given in min and cm, respectively.

When $D_X=D_Y=D_Z=0$, Eqs. (4)–(8) are a reduced version of a budding yeast cell cycle model [20,21]. Here, X represents the concentration of cyclin-dependent protein kinase (CDK): Y and Z are concentrations of two different anaphase promoting complexes (APC), APC/Cdh1 and APC/Cdc20, respectively. In Eqs. (4) and (5), m represents the cell's mass, which will be used as a primary bifurcation parameter. Equations (4)–(8) display CF bifurcations as shown in Fig. 8. For small m, Eqs. (4)–(8) also display saddle node bifurcations, a feature universal in cell cycle models [15,20]. Here, our concern is the neighborhood of CF^1 in Fig. 8. It is worth mentioning that with the increase of parameter k_2, the CF^1 bifurcation point shifts to larger m, and the distance between the right saddle node bifurcation and the CF^1 bifurcation points increases [21].

There are no experimental measurements of diffusion coefficients for CDK and APC factors. But it is known that the

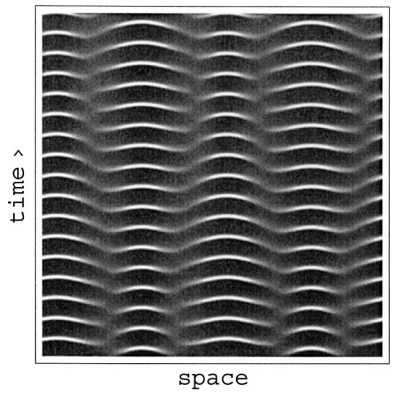

FIG. 7. Breathing periodic structures. $l=3.5$ cm; other parameters, as well as the time and space spans, are the same as in Fig. 2.

diffusion coefficient of average-sized proteins in cytoplasm is approximately $10^{-4}\mathrm{cm}^2/\mathrm{min}$ or smaller [22,23]. As our goal is a demonstration of weak turbulence in a representative model of biochemical oscillations, we choose D_X, D_Y, and D_Z arbitrarily, subject to this upper bond. For simplicity, we assume $D_Z=0$.

For simulations of Eqs. (4)–(8) we used the same method as in the previous section with $\delta t=0.05$ min, $\delta x=0.005$ cm. We found numerically that for strong perturbations, Eqs. (4)–(8) display weak turbulence, Fig. 9. Typically, for $D_X \leqslant D_Y$, we found transient, weak turbulence. When $D_X \ll D_Y$, numerical experiments indicate stationary turbulence. For instance, we simulated Eqs. (4)–(8) up to $T=10^7$ min for $m=3$, $D_X=6\times10^{-7}$ cm^2/min, $D_Y=10^{-4}$ cm^2/min, $D_Z=0$, and $l=1.28$ cm and found stationary turbulence for a number of different initial conditions. There were no qualitative changes in the weak turbulence when the CF^1 point is located away from the saddle node bifurcation, indicating that for the origin of weak turbulence in Eqs. (4)–(8), the saddle node bifurcation point is not important.

V. DISCUSSION

We have shown in this paper that two representative mathematical models of biochemical oscillations exhibiting birhythmicity—glycolytic and cell cycle models—display

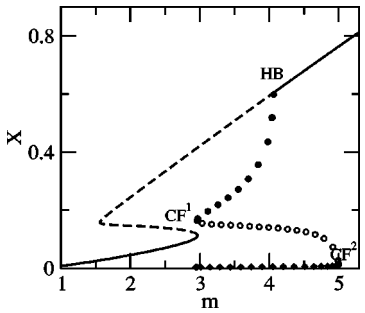

FIG. 8. Bifurcation diagram of a cell cycle model. Rate constants k_i are in units min^{-1}, $k_1=0.002$, $k_2=0.053$, $k_3=0.01$, $k_4=2$, $k_5=0.05$, $k_6=0.04$, $k_7=1.5$, $k_8=0.19$, $k_9=0.64$, $k_{10}=0.005$, $k_{11}=0.07$, and $k_{12}=0.08$. Other parameters are $P=0.15$, $J_1=0.05$, $J_2=0.01$.

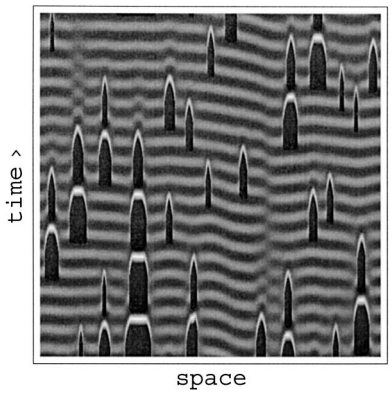

FIG. 9. Turbulence in a cell cycle model. Space time plot of Y field in Eqs. (4)–(8). The space and time spans are $L=1.28$ cm and $T=2500$ min. The pattern was obtained by recording $Y(x)$ with a time interval $\tau=5$ min.

weak turbulence (intermittency of large- and small-amplitude oscillations). We provided evidence that unstable oscillations near cyclic fold bifurcations are the mechanism of transient turbulence in birhythmic media. In the presence of wave number instability, weak turbulence is stationary.

Recently, Stich *et al.* [24,25] proposed an amplitude model for birhythmic media. An interesting question is whether the weak turbulence we discussed in this paper can be found in their model? First, let us mention two important differences between our models and the amplitude model of birhythmic media. In our case, a cyclic fold bifurcation is crucial for turbulence, but the amplitude model describes a pitchfork bifurcation of limit cycles. Second, both fast and slow oscillations in the amplitude equation are smooth, but in our case, the slow oscillations are strongly anharmonic. Besides these differences, it is well known that if phase slips develop, the CGLE generates defects [26]. Thus, these facts indicate that instead of intermittency of small- and large-amplitude oscillations, defect turbulence is likely in the amplitude model of birhythmic media. On the other hand, as far as generic patterns in birhythmic media are concern, the cell cycle model displays target patterns reminiscent of autonomous pacemakers found in the amplitude model [24,25].

To date, there is no experimental evidence of weak turbulence in glycolysis or in the cell cycle. Our results are pure theoretical predictions of mathematical models. The system sizes we simulated are much larger than the typical size of a yeast cell (10^{-3} cm). Therefore, weak turbulence is not expected in yeasts. Interestingly, some slime molds grow as syncytial plasmodia (many nuclei in a common cytoplasmic pool) that are many times larger than a typical yeast cell; cells 15 cm in diameter can be grown in the laboratory [27]. Waves of nuclear division are observed in these multinucleate plasmodia [28,29], and as we have shown, it is possible that these waves exhibit weak turbulence. Note that weak turbulence in the cell cycle would mean irregular oscillations of CDK. But for a normal cell cycle, large-amplitude oscillations of CDK are essential; CDK activity must drop below a certain threshold for nuclei to exit mitosis and divide. Therefore, hypothetically, weak turbulence in syncytial plasmodia might lead to mitotic arrest of certain nuclei in the plasmodium.

Our argument for the stability of fast oscillations against wave number instability is valid only close to the Hopf bifurcation point. Therefore, near the onset of a cyclic fold bifurcation, a more quantitative characterization of both fast and slow oscillations against wave number instability is highly desirable. Another problem for the future is to simulate wave morphologies in two spatial dimensions [30].

APPENDIX: COEFFICIENTS OF THE CGLE FOR A GLYCOLYTIC MODEL WITH SUBSTRATE INHIBITION

In this appendix, following standard procedures in Ref. [1], we will calculate coefficients of CGLE for the glycolytic model. For a convenience we assume $Q\equiv 1$ in Eqs. (1)–(3). First, let us find uniform steady-state solutions α_0 and γ_0:

$$\gamma_0 = \mu/k_s, \tag{A1}$$

$$\alpha_0 = \frac{K^4(-2\mu+\sigma)+\gamma_0^4(-2(\mu+\sigma_i)+\sigma)}{\tilde{c}} - \frac{\sqrt{-4\tilde{a}^2+4L\sigma\tilde{a}\tilde{b}+(1+\gamma_0)^2\sigma^2\tilde{b}^2}}{(1+\gamma_0)\tilde{c}}, \tag{A2}$$

where $\tilde{a}=K^4\mu+\gamma_0^4(\mu+\sigma_i)$, $\tilde{b}=(K^4+\gamma_0^4)$, and $\tilde{c}=2[K^4(\mu-\sigma)+\gamma_0^4(\mu+\sigma_i-\sigma)]$. Next we perform a linear stability analysis of (α_0,γ_0) against small fluctuations $\delta\alpha,\delta\gamma\propto\exp(iqx+i\lambda t)$. At the critical wave number $q_{cr}=0$, we obtain the characteristic equation

$$\lambda^2+(a_1+a_2+k_s)\lambda+a_1k_s=0. \tag{A3}$$

In Eq. (A3), a_1 and a_2 are given by

$$a_1 = \frac{\sigma(1+\gamma_0)^2[L+2L\alpha_0+(1+\alpha_0)^2(1+\gamma_0)^2]}{[L+(1+\alpha_0)^2(1+\gamma_0)^2]^2}, \tag{A4}$$

$$a_2 = \frac{4K^4\gamma_0^3\sigma_i}{(K^4+\gamma_0^4)^2} - \frac{2\sigma L\alpha_0(1+\alpha_0)(1+\gamma_0)}{[L+(1+\alpha_0)^2(1+\gamma_0)^2]^2}. \tag{A5}$$

Let us define a critical value for the bifurcation parameter $\sigma_i=\sigma_{i,cr}$ such that

$$a_1+a_2+k_s\equiv 0. \tag{A6}$$

Equation (A6) is the condition for a Hopf bifurcation where the characteristic equation has pure imaginary solutions, $\lambda_0=\pm i\sqrt{a_1k_s}$.

Let μ be defined by $\mu=(\sigma_i-\sigma_{i,cr})/\sigma_{i,cr}$. We develop the Jacobian matrix L of Eqs. (1)–(3) in powers of μ:

$$L = L_0+\mu L_1+\cdots. \tag{A7}$$

At $\mu=0$ the Jacobian is given by

$$L_0 = \begin{vmatrix} -a_1 & a_2 \\ a_1 & -k_s-a_2 \end{vmatrix}. \tag{A8}$$

We find the right $\mathbf{u}_0$ and left $\mathbf{u}_0^*$ eigenvectors of L_0 corresponding to λ_0:

$$\mathbf{u}_0 = \begin{pmatrix} -1+i\sqrt{\frac{k_s}{a_1}} \\ 1 \end{pmatrix}, \tag{A9}$$

$$\mathbf{u}_0^* = \frac{1}{2}\left(-i\sqrt{\frac{a_1}{k_s}},1-i\sqrt{\frac{a_1}{k_s}}\right). \tag{A10}$$

We find, further,

$$L_1 = \frac{4K^4\gamma_0^3\sigma_{i,cr}}{(K^4+\gamma_0^4)^2}\begin{vmatrix} 0 & -1 \\ 0 & 1 \end{vmatrix}. \tag{A11}$$

Let us first find c_0 in the CGLE. It is given by $c_0=\mathrm{Im}\lambda_1/\mathrm{Re}\lambda_1$, where

$$\lambda_1 = \mathbf{u}_0^* L_1\mathbf{u}_0 = \frac{2K^4\gamma_0^3}{(K^4+\gamma_0^4)^2}\sigma_{i,cr}. \tag{A12}$$

We see that λ_1 is a real number; therefore, $c_0=0$. Now following again [1], we find c_1:

$$D = \begin{vmatrix} D_\alpha & 0 \\ 0 & D_\gamma \end{vmatrix}, \tag{A13}$$

$$d'+id'' = \mathbf{u}_0^* D\mathbf{u}_0, \tag{A14}$$

$$c_1 = d''/d' = \sqrt{\frac{a_1}{k_s}}\left(\frac{D_\alpha-D_\gamma}{D_\alpha+D_\gamma}\right). \tag{A15}$$

The calculation of c_2 is a little more tedious. We need to find [1]

$$\mathbf{V}_+ = \overline{\mathbf{V}}_- = -(L_0-2\lambda_0)^{-1}\mathbf{M}_0\mathbf{u}_0\mathbf{u}_0, \tag{A16}$$

$$\mathbf{V}_0 = -2L_0^{-1}\mathbf{M}_0\mathbf{u}_0\overline{\mathbf{u}}_0, \tag{A17}$$

$$g = g'+ig'' = -2\mathbf{u}_0^*\mathbf{M}_0\mathbf{u}_0\mathbf{V}_0-2\mathbf{u}_0^*\mathbf{M}_0\overline{\mathbf{u}}_0\mathbf{V}-3\mathbf{u}_0^*\mathbf{N}_0\mathbf{u}_0^*\mathbf{u}_0^*\overline{\mathbf{u}}_0. \tag{A18}$$

The parameter c_2 in the CGLE is given by $c_2=g''/g'$. We find that $c_2=\tilde{g}''/\tilde{g}'$, where

$$\tilde{g}' = -3k_s\{k_sm_{\alpha^2}(2m_{\alpha^2}-m_{\alpha\gamma})+a_1[(2m_{\alpha^2}-m_{\alpha\gamma})(m_{\alpha^2}-m_{\alpha,\gamma}+m_{\gamma^2})-k_s(n_{\alpha^2\gamma}-3n_{\alpha^3})]+3a_1^2(n_{\alpha\gamma^2}-n_{\alpha^2\gamma}+n_{\alpha^3}-n_{\gamma^3})\}, \tag{A19}$$

$$\tilde{g}'' = \sqrt{\frac{k_s}{a_1}}\{10k_s^2m_{\alpha^2}{}^2+a_1k_s(14m_{\alpha^2}{}^2-14m_{\alpha^2}m_{\alpha,\gamma}+m_{\alpha\gamma}{}^2+10m_{\alpha^2}m_{\gamma^2}+9k_sn_{\alpha^3})+a_1^2[4(m_{\alpha^2}-m_{\alpha,\gamma}+m_{\gamma^2})^2+3k_s(n_{\alpha\gamma^2}-2n_{\alpha^2\gamma}+3n_{\alpha^3})]\}. \tag{A20}$$

In the above expressions,

$$m_{\alpha^2} = \left(\frac{\partial^2\phi(\alpha,\gamma)}{\partial\alpha^2}\right)_{\alpha_0,\gamma_0},\quad m_{\alpha\gamma} = \left(\frac{\partial^2\phi(\alpha,\gamma)}{\partial\alpha\partial\gamma}\right)_{\alpha_0,\gamma_0},$$

$$m_{\gamma^2} = \frac{2(3K^8\gamma_0^2 - 5K^4\gamma_0^6)\sigma_{i,cr}}{(K^4+\gamma_0^4)^3} - \left(\frac{\partial^2\phi(\alpha,\gamma)}{\partial\gamma^2}\right)_{\alpha_0,\gamma_0},$$

$$n_{\alpha^3} = \left(\frac{\partial^3\phi(\alpha,\gamma)}{\partial\alpha^3}\right)_{\alpha_0,\gamma_0}, \quad n_{\alpha^2\gamma} = \left(\frac{\partial^3\phi(\alpha,\gamma)}{\partial\alpha^2\partial\gamma}\right)_{\alpha_0,\gamma_0},$$

$$n_{\alpha\gamma^2} = \left(\frac{\partial^3\phi(\alpha,\gamma)}{\partial\alpha\partial\gamma^2}\right)_{\alpha_0,\gamma_0}, \quad n_{\gamma^3} = \left(\frac{\partial^3\phi(\alpha,\gamma)}{\partial\gamma^3}\right)_{\alpha_0,\gamma_0}.$$

To save space we do not present here cumbersome expressions for these derivatives.

For parameters in Fig. 1 we find that $\sigma_{i,cr}=1.282$ and $c_2 \approx 2.21$. From Eq. (A15) we see that if $D_\alpha=D_\gamma$, $c_1=0$. Therefore, $1+c_1c_2>0$ for parameters used in this paper. If $D_\alpha=0$, Eq. (A15) gives the minimal value $c_1=-0.47$. In this case, $1+c_1c_2\approx-0.03$; therefore, wave number instability is possible. However, turbulence must be weak as the parameters are very close to the stability condition $1+c_1c_2>0$ [2]. A stronger wave number instability is possible—for example, for $\mu=0.28\ \mathrm{s}^{-1}$, $K=12$, $D_\alpha=5\times10^{-7}\ \mathrm{cm}^2/\mathrm{s}$, $D_\gamma=1\times10^{-5}\ \mathrm{cm}^2/\mathrm{s}$, and other parameters are the same as in Fig. 1. In this case, we find that $\sigma_{i,cr}\approx1.095$ and $1+c_1c_2=-0.416$.

[1] Y. Kuramoto, *Chemical Oscillations, Waves and Turbulence* (Springer-Verlag, Berlin, 1984).
[2] M. C. Cross and P. C. Hohenberg, Rev. Mod. Phys. **65**, 851 (1993).
[3] Y. Kuramoto, D. Battogtokh, and H. Nakao, Phys. Rev. Lett. **81**, 3543 (1998).
[4] K. Nozaki and N. Bekki, Phys. Lett. **110A**, 133 (1985).
[5] B. I. Shraiman, A. Pumir, W. van Saarlos, P. C. Hohenberg, H. Chate, and M. Holen, Physica D **57**, 241 (1992).
[6] H. Sakaguchi, Prog. Theor. Phys. **84**, 792 (1990).
[7] I. S. Aronson and L. Kramer, Rev. Mod. Phys. **74**, 99 (2002).
[8] M. I. Rabinovich, A. B. Ezersky, and P. D. Weidman, *The Dynamics of Patterns* (World Scientific, Singapore, 2000).
[9] H. Mori and Y. Kuramoto, *Dissipative Structures and Chaos* (Springer-Tokyo, Tokyo, 1998).
[10] M. Ipsen, L. Kramer, and P. G. Sorensen, Phys. Rep. **337**, 193 (2000).
[11] J. H. Merkin, V. Petrov, S. K. Scott, and K. Showalter, Phys. Rev. Lett. **76**, 546 (1996).
[12] Y. Nishiura and D. Ueyama, Physica D **150**, 137 (2001).
[13] R. Wackerbauer and K. Showalter, Phys. Rev. Lett. **91**, 174103 (2003).
[14] A. Goldbeter, *Biochemical Oscillations and Cellular Rhythms: The Molecular Bases of Periodic and Chaotic Behavior* (Cambridge University Press, Cambridge, U.K., 1996).
[15] M. T. Borisuk and J. J. Tyson, J. Theor. Biol. **195**, 69 (2000).
[16] C. Perez-Iratxeta, J. Halloy, F. Moran, J. L. Martel, and A. Goldbeter, Biophys. Chem. **74**, 197 (1998).
[17] E. J. Doedel, A. R. Champneys, T. F. Fairgrieve, Y. A. Kuznetsov, B. Sandstede, and X. Wang, Computer code AUTO 97, Continuation and Bifurcation Software for Ordinary Differential Equations (with HomCont), 1997.
[18] A. Wolf, J. B. Swift, H. L. Swinney, and J. Vastano, Physica D **16**, 285 (1985).
[19] D. Battogtokh, Phys. Rev. E **66**, 066202 (2002).
[20] K. Chen, A. Csikasz-Nagy, B. Georffy, J. Val, B. Novak, and J. J. Tyson, Mol. Biol. Cell **11**, 369 (2000).
[21] D. Battogtokh and J. J. Tyson, Chaos (to be published).
[22] J. W. Wojcieszyn, R. A. Schlegel, E. S. Wu, and K. A. Jacobson, Proc. Natl. Acad. Sci. U.S.A. **78**, 4407 (1981).
[23] G. Zubay, *Biochemistry* (Addison-Wesley, Reading, MA, 1983).
[24] M. Stich, M. Ipsen, and A. S. Mikhailov, Phys. Rev. Lett. **86**, 4406 (2001).
[25] M. Stich, M. Ipsen, and A. S. Mikhailov, Physica D **171**, 19 (2002).
[26] H. Chate, Nonlinearity **7**, 185 (1994).
[27] J. Mohberg and H. P. Rusch, J. Bacteriol. **97**, 1411 (1969).
[28] E. F. Haskins (unpublished).
[29] B. Novak and J. J. Tyson, J. Theor. Biol. **165**, 101 (1993).
[30] Our preliminary results show the existence of weak turbulence in dimension 2.